Bioresource Technology 352 (2022) 127041

Contents lists available at ScienceDirect

Bioresource Technology

journal homepage: www.elsevier.com/locate/biortech

Chemometric optimisation of enzymatic hydrolysis of beechwood xylan to target desired xylooligosaccharides

Gloria L. Díaz-Arenas [a,b,c], Leo Lebanov [d,e], Estrella Sanz Rodríguez [d,e], M. Munir Sadiq [c], Brett Paull [d,e], Gil Garnier [a,b,c], Joanne Tanner [a,b,c,*]

[a] Bioresource Processing Research Institute of Australia (BioPRIA), Department of Chemical and Biological Engineering, Monash University, Clayton, VIC 3800, Australia
[b] ARC Industrial Transformation Research Hub for Processing Advanced Lignocellulosics (PALS), Department of Chemical and Biological Engineering, Monash University, Clayton, VIC 3800, Australia
[c] Department of Chemical and Biological Engineering, Monash University, Clayton, VIC 3800, Australia
[d] Australian Centre for Research on Separation Science (ACROSS), School of Natural Sciences, University of Tasmania, Hobart, TAS 7001, Australia
[e] ARC Industrial Transformation Research Hub for Processing Advanced Lignocellulosics (PALS), School of Natural Sciences, University of Tasmania, Hobart, TAS 7001, Australia

HIGHLIGHTS

- Enzymatic hydrolysis of beechwood xylan to produce XOS using endoxylanase.
- Identification of 22 linear and branched XOS by HPAEC-QqQ-MS.
- Prediction of hydrolysis parameters by a comprehensive computational modelling set.
- The pH as the dominant factor influencing xylan hydrolysate yield and composition.

GRAPHICAL ABSTRACT

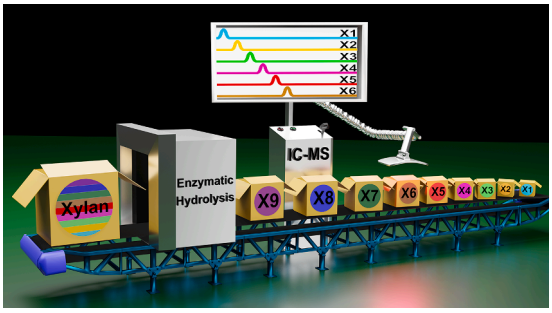

ARTICLE INFO

Keywords:
Endoxylanases
Enzymatic hydrolysis
Mass Spectrometry
Xylan, Xylooligosaccharides

ABSTRACT

Generation of specific xylooligosaccharides (XOS) is attractive to the pharmaceutical and food industries due to the importance of their structure upon their application. This study used chemometrics to develop a comprehensive computational modelling set to predict the parameters maximising the generation of the desired XOS during enzymatic hydrolysis. The evaluated parameters included pH, temperature, substrate concentration, enzyme dosage and reaction time. A Box-Behnken design was combined with response surface methodology to develop the models. High-performance anion-exchange chromatography coupled with triple-quadrupole mass spectrometry (HPAEC-QqQ-MS) allowed the identification of 22 XOS within beechwood xylan hydrolysates. These data were used to validate the developed models and demonstrated their accuracy in predicting the parameters maximising the generation of the desired XOS. The maximum yields for X2-X6 were 314.2 ± 1.2, 76.6 ± 4.5, 38.4 ± 0.4, 17.8 ± 0.7, and 5.3 ± 0.2 mg/g xylan, respectively. These values map closely to the model predicted values 311.7, 92.6, 43.0, 16.3, and 4.9 mg/g xylan, respectively.

* Corresponding author at: Bioresource Processing Research Institute of Australia (BioPRIA), 15 Alliance Lane, Monash University, Clayton, VIC, Australia.
E-mail address: joanne.tanner@monash.edu (J. Tanner).

https://doi.org/10.1016/j.biortech.2022.127041
Received 7 February 2022; Received in revised form 16 March 2022; Accepted 17 March 2022
Available online 19 March 2022

1. Introduction

The agriculture and forestry industries, following global sustainability principles, have recently given more attention to the complete utilisation of lignocellulosic biomass and its conversion into high-value products (Li et al., 2019). Among those, xylooligosaccharides (XOS) are especially attractive for their appeal in the pharmaceutical, phytopharmaceutical, and food industries, with a growing global demand expected to reach US $130 million by 2025 (Santibáñez et al., 2021). XOS with different degrees of polymerisation (DP) are generated from xylan and made of β-D-xylopyranosyl residues connected by β-(1→4)-xylosidic linkages (Samanta et al., 2015). The applications of XOS are determined by their DP, type and number of substituents. Low DP XOS such as xylobiose (X2), xylotriose (X3) and xylotetraose (X4), have potential applications as prebiotics, anti-microbials, and anti-inflammatory agents (Moure et al., 2006). XOS with DP greater than four can be used as food ingredients, stabilisers, thickeners and emulsifiers (Gonçalves De Oliveira et al., 2021). In addition to the DP, the XOS properties can be influenced by the number and type of branches, which are ultimately determined by the xylan source (Naidu et al., 2018). Xylan can be obtained from hardwoods (glucuronoxylans), softwoods (arabino-glucuronoxylans), seaweeds (homoxylans), starch, seeds (arabinoxylans), grasses, and cereals (glucuronoarabinoxylans) (Santibáñez et al., 2021). Among these, hardwood is one of the richest sources of xylan, and abundant hardwood biomass is a residue of the forestry, pulp and paper industries (Guo et al., 2020).

Enzymatic hydrolysis is preferred over chemical hydrolysis to convert xylan into XOS as it eliminates the use of corrosive chemicals, is performed at mild conditions, reduces the generation of monomers, and does not produce undesirable by-products (Aachary and Prapulla, 2011; Akpinar et al., 2007). During this process, enzymes termed endoxylanases (EC 3.2.1.8) hydrolyse the β-(1→4) linkages of the xylan backbone, converting it into XOS of different DP (Bragatto et al., 2013). Xylanases are classified into several families of glycosyl hydrolases (GH). Xylanases from GH11 are known as endoxylanases as they preferentially attack the main backbone and show a low action at the non-reducing end (Linares-Pasten et al., 2017). This G11 feature is ideal to minimise the production of xylose (X1), which can inhibit the xylanase activity when present in high concentrations (Rahmani et al., 2019).

The key parameters in the enzymatic hydrolysis of xylan influencing the XOS yield and composition are: 1) pH of the reaction medium, 2) incubation temperature, 3) substrate concentration (mg xylan/mL solution), 4) enzyme dosage (U/mL solution), and 5) reaction time (Li et al., 2020; Santibáñez et al., 2021). Defining and controlling these parameters are crucial steps to tailor the production of XOS with various DP. In addition, the yield and composition of xylan hydrolysates are also influenced by the xylan source (Bragatto et al., 2013; Chapla et al., 2012). Therefore, enzymatic hydrolysis of each xylan source must be optimised separately.

The detailed and accurate structural characterisation of XOS is critical to this optimisation and has been conventionally carried out in two steps. In the initial step, the xylan hydrolysates are fractionated by a chromatographic technique such as size exclusion chromatography (SEC), gel filtration chromatography (GFC), reversed-phase high-performance liquid chromatography (RP-HPLC), thin-layer chromatography (TLC), or high-performance anion-exchange chromatography (HPAEC) (Bhatia et al., 2020; Brenelli et al., 2020; Li et al., 2016; Moniz et al., 2014). The last one can provide the highest selectivity and resolution in separating oligosaccharides (Kabel et al., 2002; Sanz Rodriguez et al., 2020). The second step relies on an off-line molecular characterisation technique, such as nuclear magnetic resonance (NMR), Fourier transform infrared spectroscopy (FT-IR), matrix-assisted laser desorption ionisation mass spectrometry (MALDI-MS), or electrospray ionisation mass spectrometry (ESI-MS), to identify the separated compounds present in the hydrolysate (Bowman et al., 2012; Kabel et al., 2003; Li et al., 2016). Recently, a facile, fast, selective, and sensitive method based on on-line coupling between HPAEC and triple-quadrupole mass spectrometry (QqQ-MS) has been developed (Sanz Rodríguez et al., 2022). This method allows the separation and identification of linear and branched XOS in one workflow without the need for extra fractionation and desalting steps for MS detection, and/or additional techniques for XOS characterisation such as NMR or FT-IR.

This study aimed at developing computational models to optimise and control the generation of XOS via enzymatic hydrolysis of xylan. A Box-Behnken design including forty-eight experiments was used to chemometrically evaluate the effects of pH, incubation temperature, substrate concentration, enzyme dosage, and reaction time on xylan hydrolysate composition and yield. To develop the models, beechwood xylan (glucuronoxylan) was hydrolysed using *endo*-1,4-β-xylanase from *Thermomyces lanuginosus*. The generated XOS were characterised using high-performance anion-exchange chromatography coupled with triple-quadrupole mass spectrometry (HPAEC-QqQ-MS) and the extensive data set was analysed using response surface methodology (RSM). The optimised model parameters were cross-validated experimentally and the models were used to maximise the generation of desired XOS, enabling their commercial production by reducing the cost of downstream purification.

2. Materials and methods

2.1. Chemicals and reagents

Xylan from beechwood (*Fagus sylvatica L.*) was obtained from Apollo Scientific (Cheshire, UK). Citric acid monohydrate, sodium citrate dihydrate, glucose (99.5%), arabinose (99%), glucuronic acid (98%), acetic acid (99.8%), xylose (X1, 99%), calcium carbonate (≥ 99.0%), and *endo*-1,4-β-xylanase from *Thermomyces lanuginosus* (≥ 2500 U/g) were purchased from Sigma-Aldrich (St Louis, USA). Enzyme activity (U) is defined as the amount of enzyme required to produce 1 μmol of reducing sugar equivalents (X1) per minute. Sulphuric acid (98%), sodium hydroxide (NaOH) 50% w/w solution in extra pure water, and sodium acetate (NaOAc) salt electrochemical-grade were purchased from Thermo Fisher Scientific (Sunnyvale, USA) and used to prepare HPAEC eluents. Methanol (MeOH) from Honeywell Burdick & Jackson (Muskegon, USA), and lithium chloride (LiCl, ≥ 99%) from Sigma-Aldrich (St Louis, USA) were utilised to prepare the MS make-up solution. De-ionised water (DIW) was obtained from a Millipore Milli-Q water purification system (Bedford, USA). Carbon-13-labelled levoglucosan (1,6-anhydro-β-D-glucopyranose, U-13C6, 98%) from Cambridge Isotope Laboratories Inc, (Tewksbury, USA) was used as an internal standard (IS). Xylobiose (X2), xylotriose (X3), xylotetraose (X4), xylopentaose (X5), and xylohexaose (X6) with purity > 95% were obtained from Megazyme (Bray, Ireland). Individual stock solutions of X1-X6 (1000 mg/L for X1, 2000 mg/L for X2 and 500 mg/L for X3-X6) were prepared by dissolving the appropriate amount of each compound in DIW. The target analytes were quantified using an internal standard calibration method. Intermediate solutions to plot 6-point calibration curves were prepared by diluting the stock solutions at different concentrations and adding a fixed amount of internal standard (20 mg/L). Quantitative results, expressed as yield (Eq. (1)), were obtained for X1-X6 in xylan hydrolysates using the calibration curves from the commercial standards. For the rest of the linear (> X6) and branched XOS in the hydrolysates, pseudo-quantitative results were obtained by comparing the peak area$_{XOS}$/peak area$_{IS}$, due to the unavailability of commercial standards. Nonetheless, their identity was confirmed using high-resolution-accurate mass Orbitrap mass spectrometry (HRAM-Orbitrap-MS).

$$\text{Yield} = \frac{\text{XOS (DP1} - 6\text{) in hydrolysate (mg)}}{\text{Xylan (g)}} \quad (1)$$

2.2. Determination of xylan composition

The composition of beechwood xylan was determined following the National Renewable Energy Laboratory (NREL) analytical procedure (Sluiter et al., 2008). In brief, a two-step acid hydrolysis was conducted in triplicate to convert xylan into its constituent monomers starting with 72% sulfuric acid pre-hydrolysis at 30 °C for 1 h. Subsequently, the acid was diluted to 4% and the hydrolysis was conducted at 121 °C for 1 h. The samples were neutralised using calcium carbonate and centrifuged (Thermo Scientific Sorvall LYNX 4000, Waltham, USA) at 10,000 rpm for 5 min. The supernatant was passed through 0.2 μm Acrodisc® syringe filter with Supor® membrane (Pall Corporation, Port Washington, USA) prior to monosaccharide composition analysis. The analysis was conducted in an Agilent 1260 Infinity ll HPLC system coupled with a refractive index detector, and the carbohydrates separation was performed via an Agilent Hi-Plex H (300 × 7.7 mm) chromatographic column (Agilent Technologies, Santa Clara, USA). The column was set at 60 °C in isocratic elution mode with 5 mM sulfuric acid at a flow rate of 0.7 mL/min for 50 min. The calibration was performed using a range of monomeric sugars (xylose, glucose and arabinose), and glucuronic and acetic acids.

2.3. Design of experiments

The enzymatic hydrolysis of beechwood xylan was carried out following the conditions determined by the Box-Behnken design of experiments (see supplementary material). Forty-eight experiments were randomly conducted to evaluate three coded levels (-1, 0, and + 1) of five independent variables including pH, incubation temperature, reaction time, enzyme dose, and xylan concentration. The experimental design was carried out in two blocks and the central coded levels were repeated six times to estimate the standard error of the experiments.

2.4. Enzymatic hydrolysis

The enzymatic hydrolysis of the beechwood xylan was conducted using *endo*-1,4-β-xylanase and 50 mM sodium citrate buffer. The desirable xylan concentration and enzyme dose were mixed with 10 mL of buffer at a specific pH (reaction mixture). The mixture was placed in an incubator shaker (Infors Ecotron, Bottmingen, Switzerland) at 250 rpm for a certain time at a specific temperature. The parameters studied here were pH of buffer (4.0, 5.5, and 7.0), xylan concentration (1, 2, and 3% w/v), enzyme dose (50.0, 62.5, and 75.0 U/mL of reaction mixture equivalent to 20, 25, and 30 mg of enzyme per mL of reaction mixture, respectively), reaction time (30, 60, and 90 min) and incubation temperature (25.0, 37.5, and 50.0 °C). The levels of parameters were established based on the range at which xylanase is active (Linares-Pasten et al., 2017), and the reported data on enzymatic hydrolysis of different xylan sources (Chapla et al., 2012; Singh et al., 2018). Upon completion of the reaction time, the reaction was terminated by immersing the samples in a boiling water bath for 10 min. This approach has been proven to stop enzyme activity (Bhatia et al., 2020; Ghosh et al., 2021). Next, the samples were immediately centrifuged at 10,000 rpm and 20 °C for 5 min. The supernatant was removed using a Pasteur pipette, filtered by a 0.2 μm syringe filter, and transferred to a conical tube for storage at 4 °C. The bicinchoninic acid (BCA) assay was conducted on the filtered samples to measure the enzyme concentration using the Novagen® BCA Protein Assay Kit (Merck Millipore, Darmstadt, Germany) following the manufacturer's instructions. In brief, the two reagents, BCA solution and 4% cupric sulfate, were mixed in a 50:1 ratio and 200 μL were added to 25 μL of sample in a 96-well plate. The plate was shaken for 30 s before incubation at 37 °C for 30 min. After incubation, the plate was immediately placed into a microplate reader (Infinite 200 pro, Tecan, Switzerland) and the absorbance was read at 562 nm. Bovine serum albumin (0–1000 μg/mL) was used as the calibration standard and all measurements were conducted in triplicate.

2.5. Instrumental parameters and analytical method

A Thermo Scientific Dionex ICS-5000$^+$ Reagent-Free IC (RFIC) system coupled to a Thermo Scientific TSQ Quantiva triple-stage quadrupole mass spectrometer, equipped with an Ion Max NG source operating in heated-Electro Spray Ionisation (H-ESI) mode, was used throughout. Hydrolysate samples were diluted with deionised water and mixed with an internal standard (20 mg/L) before analysis using HPAEC-QqQ-MS, following the method previously developed (Sanz Rodríguez et al., 2022). Briefly, 20 μL of each diluted sample were injected via an AS-AP autosampler (controlled temperature at 21 °C) to the coupled Dionex AminoTrap (3 × 50 mm) and CarboPac PA200 analytical column (3 × 250 mm). Target solutes were separated at 35 °C using a gradient from 2 to 150 mM NaOAc (eluent B) over 30 min combined with 150 mM NaOH (eluent A). The flow rate was set at 0.45 mL/min within a total run time of 60 min, including a short cleaning step to elute strongly retained compounds and an equilibrating step before the next injection. An anion self-regenerating Dionex ADRS 600 suppressor (4 mm) was placed in-line after the column, which electrolytically converted the NaOH eluent to water and NaOAc eluent to acetic acid. The suppressor was run in external-regenerating mode using an AXP pump to deliver 3 mL/min DIW. LiCl at 0.5 mM in MeOH was added using a second auxiliary pump at a flow rate of 0.05 mL/min to assist the ionisation at the ESI source and enhance the response for XOS via monitoring their positive lithium adducts. The acquisition was performed in full-scan mode over the range of m/z 100–1800. All instrumentation, columns and suppressor were from Thermo Fisher Scientific (San Jose, USA). Instrument control, data acquisition and processing were via *Chromeleon 7* Software, version 7.2.6.

2.6. Response surface methodology

Response surface methodology (RSM) is a statistical technique aimed at establishing a mathematical relationship between the response variables and a set of independent variables. Based on this relationship, it is possible to predict the level of the independent variables that will result in the maximum or minimum value of the response of interest (Khuri and Mukhopadhyay, 2010). Herein, the response variables were defined as the maximum or minimum amount of the identified XOS. The quantitative (yields) and pseudo-quantitative (peak $area_{XOS}$/peak $area_{IS}$) results, obtained experimentally following the Box-Behnken design, were used to create the full-quadratic RSM models (Eq. (2)) generated by "*rsm*" Package in R software (R.3.4.4) (Lenth, 2009).

$$y = \beta_0 + \sum_{i=1}^{5} \alpha_i x_i + \sum_{i=1}^{5} \sum_{j=1}^{5} \alpha_{ij} x_i x_j (i \le j) \quad (2)$$

In this equation, y is the response variable, β_0 is the intercept, and a_i, a_{ii} and a_{ij} are the coefficients of the linear, quadratic, and interaction parameters, respectively. The independent variables are represented as $x(x_i, x_j)$. The parameters leading to the maximum generation of each identified XOS were determined based on the developed RSM models.

The goodness-of-fit of the RSM models was evaluated by the determination coefficient (R^2), adjusted determination coefficient (adjusted-R^2), and lack of fit (Sutay Kocabaş et al., 2021). Statistical significance of the linear, quadratic, and interaction terms were examined by one-way analysis of variance (ANOVA). The relative error of prediction (REP) was calculated using Eq. (3);

$$\mathrm{REP}(\%) = 100 \sqrt{\frac{\sum_{i=1}^{n} (C_i - C_i^{'})^2}{\sum_{i=1}^{n} C_i^2}} \quad (3)$$

where C_i and $C_i^{'}$ are the actual and predicted values for the response variable in sample i, respectively. In all evaluations, $P < 0.05$ was

Table 1
Species attributed to lithium adducts $[M+Li]^+$ and $[M+2Li]^{2+}$ of linear and branched XOS obtained by HPAEC-QqQ-MS.

Peak no.	Compound	Molecular formula	Monoisotopic mass (Da)[a]	HPAEC-QqQ-MS[b] $[M+Li]^+$ (m/z)	$[M+2Li]^{2+}$ (m/z)	Retention time (min)
1	X1	$C_5H_{10}O_5$	150.0528	**157.07**	n.d.[c]	3.78
2	X2	$C_{10}H_{18}O_9$	282.0951	**289.11**	n.d.[c]	4.19
3	X3	$C_{15}H_{26}O_{13}$	414.1374	**421.15**	n.d.[c]	4.96
4	X4	$C_{20}H_{34}O_{17}$	546.1797	**553.20**	n.d.[c]	6.38
5	X5	$C_{25}H_{42}O_{21}$	678.2220	**685.24**	n.d.[c]	8.15
6	X6	$C_{30}H_{50}O_{25}$	810.2643	**817.28**	n.d.[c]	9.74
7	X7	$C_{35}H_{58}O_{29}$	942.3065	**949.32**	478.17	11.20
8	X8	$C_{40}H_{66}O_{33}$	1074.3488	1081.36	**544.19**	12.77
9	X9	$C_{45}H_{74}O_{37}$	1206.3911	1213.41	**610.21**	14.15
10	X2MeGluA	$C_{17}H_{28}O_{15}$	472.1429	**479.16**	n.d.[c]	12.90
11	X3MeGluA	$C_{22}H_{36}O_{19}$	604.1852	**611.20**	n.d.[c]	10.89
12	X4MeGluA	$C_{27}H_{44}O_{23}$	736.2275	**743.24**	n.d.[c]	11.76
13	X5MeGluA	$C_{32}H_{52}O_{27}$	868.2697	**875.29**	441.15	13.15
14	X6MeGluA	$C_{37}H_{60}O_{31}$	1000.3120	**1007.33**	507.17	14.57
15	X7MeGluA	$C_{42}H_{68}O_{35}$	1000.3120	**1139.37**	573.19	15.83
16	X8MeGluA	$C_{47}H_{76}O_{39}$	1264.3966	1271.41	**639.21**	17.00
17	X9MeGluA	$C_{52}H_{84}O_{43}$	1396.4389	1403.45	**705.24**	18.12
18	X10MeGluA	$C_{57}H_{92}O_{47}$	1528.4811	1535.50	**771.26**	19.26
19	X11MeGluA	$C_{62}H_{100}O_{51}$	1660.5234	n.d.[c]	**837.28**	20.21
20	X7MeGluA2	$C_{49}H_{78}O_{41}$	1322.4021	1329.42	**668.22**	21.65
21	X8MeGluA2	$C_{54}H_{86}O_{45}$	1454.4444	n.d.[c]	**734.24**	22.46
22	X9MeGluA2	$C_{59}H_{94}O_{49}$	1586.4866	n.d.[c]	**800.26**	23.32

[a] Exact mass calculated using the mass of the most abundant isotope of each element.
[b] Species that provided the highest response are in bold.
[c] not detected.

considered to be statistically significant. The mean error of prediction (MEP) was calculated following the Eq. (4) where n is the number of samples.

$$\mathrm{MEP} = \frac{\sum_{i=1}^{n} |C_i - C_i^{'}|}{n} \quad (4)$$

To verify the RSM models, a new set of experiments following the parameters determined for X1-X6 was conducted in triplicate, and the Bland-Altman plot with 95% limits of agreement was developed to compare the predicted and experimental results.

2.7. Principal component analysis

Herein, PCA was conducted to reduce the number of independent variables and explore their contribution to diversification among the samples. The experimentally obtained quantitative and pseudo-quantitative data, according to the Box-Behnken design, were pre-processed by mean centring and scaling by range, and subjected to PCA using MetaboAnalyst 5.0 online software (Pang et al., 2021) and the "*mdatools*" Package in R software (R.3.4.4) (Kucheryavskiy, 2020).

3. Results and discussion

3.1. Analysis of the xylan hydrolysates using HPAEC-QqQ-MS

Enzymatic hydrolysis is the preferred method to convert xylan into XOS due to the low by-product generation and mild reaction conditions required (Aachary and Prapulla, 2011). The monosaccharide composition of the beechwood xylan was determined following the NREL procedure. Xylose was the predominant component accounting for 79.9 ± 1.1% of the total carbohydrates, followed by 9.5 ± 0.8% glucuronic acid, 8.4 ± 0.4% glucose, 1.9 ± 0.2% arabinose, and 0.3 ± 0.1% acetic acid. The enzymatic hydrolysis of the xylan using xylanase from *Thermomyces lanuginosus* was performed applying the parameters assigned using the Box-Behnken design of experiments. The BCA assay showed that the centrifugation and filtration succeeding the hydrolysis removed 52.9 ± 1.9%, 65.1 ± 4.1, and 69.0 ± 4.1% of the enzyme from the hydrolysate samples with initial enzyme dose of 20, 25, and 30 mg/mL, respectively. The hydrolysate samples were analysed using HPAEC-QqQ-MS applying the method previously developed (Sanz Rodríguez et al., 2022). Table 1 details the 22 compounds identified in the hydrolysate samples including their name abbreviations, molecular formulae, theoretical monoisotopic masses, experimental m/z values for the lithium adducts generated at the ESI source, and retention times.

The main signals observed were for singly charged lithium adducts $[M+Li]^+$ for XOS with molecular weight lower than ~ 800 Da, while an additional signal corresponding to the $[M+2Li]^{2+}$ adducts were also detected for XOS with molecular weight above ~ 800 Da. The $[M+2Li]^{2+}$ species either presented a higher response or was the only signal detected for some of the XOS. Both species are presented in Table 1, and the primary species detected for each compound is marked in bold. The identity of X1 to X6 was confirmed by comparing the mass spectra of the cationised species and the retention times with those obtained from the commercial standards. Since commercial standards were unavailable for the remaining XOS (i.e. Table 1 No. 7–22), their identity was confirmed using HRAM-Orbitrap-MS, as detailed elsewhere (Sanz Rodríguez et al., 2022).

The identified XOS included linear X1 to X9, and branched X2 to X11, with one or two 4-*O*-methyl-D-glucuronic acid (MeGluA) substituents. > 90% of hemicellulose from hardwood is comprised of glucuronoxylan with MeGluA substituents in the main backbone (Santibáñez et al., 2021). XOS with MeGluA substituents have shown higher antioxidant activity compared to their linear counterparts, which is correlated with their molar ratio (Valls et al., 2018). These XOS offer a natural source of antioxidants and a sustainable alternative to synthetic food additives (Taghvaei and Jafari, 2015). When glucuronoxylan is depolymerised, the ratio of the generated XOS to MeGluA can vary depending on the species and part of the plants from which xylan is extracted (Ebringerová, 2005). For example, the ratio of XOS to MeGluA was identified as 1:1 and 7:1 in *Eucalyptus globulus* (Reis et al., 2005), and between 5:1 to 16:1 in beechwood, (Wei et al., 2021). The ratio of XOS to MeGluA identified in this study complements the previous studies and ranged from 2:1 to 11:1.

As shown in Table 1, there was a linear increment in the retention time with increasing DP for linear (i.e. No. 1–9) and branched XOS (i.e.

Table 2
Analysis of variance (ANOVA) and figures of merits for the response surface methodology (RSM) models for the 22 identified XOS.

Response Variables	R^2	Adjusted-R^2	REP (%)	MEP	*F* value*	*P*-value
Quantification, mg/L						
X1	0.98	0.963	9.70	2.08×10^{0}	61.86	2.2×10^{-16}
X2	0.98	0.963	4.62	1.63×10^{1}	62.59	2.2×10^{-16}
X3	0.95	0.905	8.75	8.96×10^{0}	23.35	3.6×10^{-12}
X4	0.94	0.897	18.78	3.67×10^{0}	21.52	9.9×10^{-12}
X5	0.97	0.941	15.80	1.44×10^{0}	38.51	6.8×10^{-15}
X6	0.96	0.936	17.30	5.00×10^{1}	35.59	1.9×10^{-14}
Peak area XOS/ Peak area IS						
X7	0.93	0.870	20.99	3.00×10^{-3}	16.77	2.0×10^{-10}
X8	0.92	0.862	26.05	8.64×10^{-5}	15.73	4.3×10^{-10}
X9	0.84	0.720	37.82	4.10×10^{-4}	7.04	2.9×10^{-6}
X2MeGluA	0.93	0.885	10.88	5.50×10^{-3}	19.10	4.2×10^{-11}
X3MeGluA	0.96	0.926	7.68	4.20×10^{-2}	30.34	1.4×10^{-13}
X4MeGluA	0.94	0.893	8.49	4.40×10^{-1}	20.56	1.7×10^{-11}
X5MeGluA	0.95	0.907	9.08	2.27×10^{-1}	23.88	2.8×10^{-12}
X6MeGluA	0.97	0.945	10.48	3.70×10^{-2}	41.60	2.5×10^{-15}
X7MeGluA	0.95	0.907	20.99	1.20×10^{-2}	23.99	2.6×10^{-12}
X8MeGluA	0.89	0.812	30.54	8.50×10^{-3}	11.16	2.2×10^{-8}
X9MeGluA	0.92	0.866	25.73	4.64×10^{-3}	16.19	3.0×10^{-10}
X10MeGluA	0.88	0.798	31.78	2.40×10^{-3}	10.30	5.3×10^{-8}
X11MeGluA	0.87	0.781	33.19	1.20×10^{-3}	9.38	1.5×10^{-7}
X7MeGluA2	0.89	0.815	10.69	2.20×10^{-2}	11.32	1.9×10^{-8}
X8MeGluA2	0.93	0.885	11.46	1.10×10^{-2}	19.07	4.3×10^{-11}
X9MeGluA2	0.64	0.381	47.41	6.40×10^{-3}	2.45	1.6×10^{-2}

R^2: correlation coefficient; adjusted-R^2: Adjusted correlation coefficient; REP: relative error of prediction; MEP: mean error of prediction; *F*-value: statistic of Fisher. *Degrees of freedom numerator and denominator (20,27); All terms were considered in the equations.

Table 3
Predicted values of the enzymatic hydrolysis parameters obtained by response surface methodology (RSM) models to generate the maximum amount of XOS.

No.	Compound	pH	Temp (°C)	Time (min)	Enzyme (U/mL)	Xylan (% w/v)
1	X1	7.0	50	90	75	3
2	X2	7.0	25	30	75	3
3	X3	4.5	25	30	75	3
4	X4	4.0	25	30	75	3
5	X5	4.0	25	30	75	3
6	X6	4.0	25	30	75	3
7	X7	4.0	25	90	55	3
8	X8	4.0	25	30	75	3
9	X9	4.0	35	90	55	3
10	X2MeGluA	7.0	50	90	75	3
11	X3MeGluA	7.0	50	90	75	3
12	X4MeGluA	7.0	50	90	55	3
13	X5MeGluA	4.5	50	90	75	3
14	X6MeGluA	4.0	25	40	75	3
15	X7MeGluA	4.0	25	30	75	3
16	X8MeGluA	4.0	25	90	55	3
17	X9MeGluA	4.0	25	90	55	3
18	X10MeGluA	4.0	25	90	55	3
19	X11MeGluA	4.0	25	90	55	3
20	X7MeGluA2	7.0	50	90	75	3
21	X8MeGluA2	4.0	37	90	75	3
22	X9MeGluA2	4.0	25	30	75	3

No 11–22), except for the branched X2MeGluA (i.e. No. 10), which was eluted after X3MeGluA and X4MeGlu. Mechelke *et al.* observed similar behaviour in the retention time, where linear and non-linear correlations between DP and retention time were obtained for linear XOS and branched arabinoxylooligosaccharides, respectively (Mechelke et al., 2017). HPAEC is based on the use of high pH tolerant pellicular anion-exchange resin columns to perform the high resolution carbohydrate separation required (Sanz Rodríguez et al., 2022). At a high pH, linear XOS with pKa values in the range of 12–14 are partially ionised and thus can be separated by an anion-exchange mechanism (Rocklin and Pohl, 1983). For branched XOS, the acidic groups or other sugar decorations likely interact with the stationary phase of the CarboPac PA200 resin through secondary mechanisms affected by the size, position of decoration, or type of linkage. These could explain the non-linear correlation between DP and retention time observed for X2MeGluA.

3.2. Response surface methodology

The DP, and type and degree of substitution determine the chemical and biological properties of XOS (Moure et al., 2006; Santibáñez et al., 2021). In this study, 22 XOS with different DP, and types and degrees of substitution were generated through the enzymatic hydrolysis of xylan. Finding the optimum values for the key parameters involved in the generation of XOS including pH, incubation temperature, reaction time, enzyme dose, and xylan concentration is crucial to controlling the enzymatic reaction and targeting the desired compounds. As a result, 22 RSM models were developed in this study to find the value of parameters leading to the maximum or minimum amount of each identified XOS (i.e. the response variables). Extracted ion chromatograms (EICs) of the main lithium adduct formed at the ESI source (Table 1) were used to obtain quantitative (X1-X6 yields) and pseudo-quantitative (peak area$_{XOS}$/peak area$_{IS}$) results to create the RSM models (see supplementary material). Table 2 shows the R^2, adjusted-R^2, relative error of prediction (REP), mean error of prediction (MEP), and the *P*-values calculated by analysis of variance (ANOVA) to evaluate the goodness-of-fit for these models. The R^2 and adjusted-R^2 for X1-X6 were above 0.89 with REP values below 18.80%, indicating a high correlation between these models and the experimental data. The R^2 and adjusted-R^2 obtained for the models of larger DP for both linear ($\geq$ X7) and branched XOS were above 0.72 except for X9MeGluA2. Some of these XOS were only generated at certain parameter values, which resulted in a limited

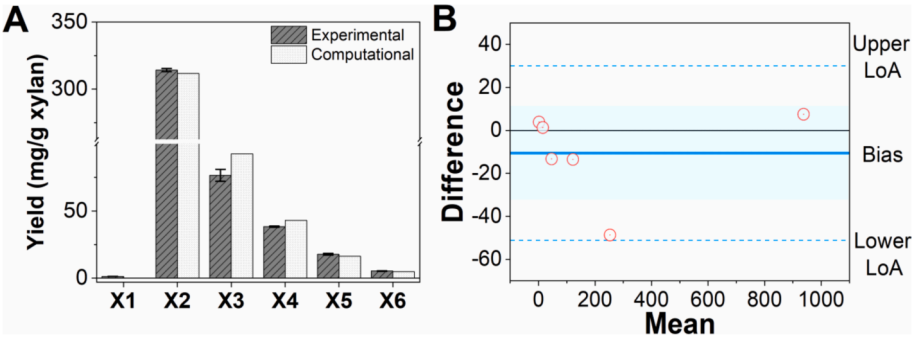

Fig. 1. (A) The computational yields of X1-X6 predicted by the response surface methodology (RSM) models vs the experimental results obtained by HPAEC-QqQ-MS, (B) Bland–Altman plot depicting the difference between the experimental and predicted yields obtained from the RSM models for X1 to X6. The solid bold line represents the bias and the dashed lines are 95% upper and lower limits of agreement (LoA).

number of data points available to create the RSM models. However, *P*-values in all the developed models were lower than 0.05, implying that the models were statistically significant.

3.2.1. Optimal conditions to maximise the generation of XOS

Based on the developed RSM models, the hydrolysis parameters resulting in the maximum amount for each identified XOS were determined and are presented in Table 3. ANOVA was employed to calculate the *P*-values of the individual linear, quadratic, and interactions of the evaluated parameters with influence on the response variables (see supplementary material). For the linear XOS, the only linear and quadratic factor presenting a *P*-value below 0.05 was pH, indicating its significance in the generation of X1 to X9. In the case of interactions, pH and xylan concentration appeared to be the common factor significantly influencing the generation of X1 to X9, except for X3 ($P > 0.05$). The other interactions with significant influence on the generation of linear XOS were pH and temperature for X2, X5, X6, and X8, enzyme dose and xylan concentration for X2, X3, and X4, and pH and time for X2. For the branched XOS, both pH and xylan concentration were the parameters with linear, quadratic, and interaction terms that had a significant effect on the amount of the majority of branched XOS. It can be inferred that, within the range of the parameters evaluated, pH 4.0 consistently led to the production of the 22 identified linear and branched XOS. In contrast, at pH 7.0, no linear XOS with DP > 4 nor branched XOS with DP > 8 were produced (see supplementary material). Interestingly, the highest evaluated level of xylan concentration, 3% w/v, was the optimal level for the generation of the 22 XOS.

Endo-1,4-β-xylanase from *Thermomyces lanuginosus* which possesses a low β-xylosidase activity was used in this study (Ghosh et al., 2021; Polizeli et al., 2005). This xylanase is classified into the GH11 family, which hydrolyses the internal β-(1→4)-xylosidic linkages of xylan via the nucleophile and catalytic acid/base glutamic acid residues (Linares-Pasten et al., 2017; Soliman et al., 2009). The two glutamic acids at the enzyme's active site must be ionised for the catalysis to happen (Chadha et al., 2019; Xu et al., 2013). This makes the pH of the reaction medium a determinant factor in the xylanase catalytic activity, as confirmed in this work. The nucleophile and catalytic acid/base glutamic acid residues of the xylanase extracted from *Bacillus circulans* (GH11) have pKa of 4.6 and 6.7, respectively (Joshi et al., 2008). As a result, the enzyme is expected to show an enhanced activity at neutral and basic pH. This is supported by the HPAEC-QqQ-MS analysis presented here, where the yields of X1 and X2 considerably increased when the pH was elevated from 4.0 to 7.0 and all other parameters held constant. For example, changing the pH from 4.0 to 7.0 at temperature 50 °C, reaction time 60 min, enzyme dose 62.5 U/mL, and xylan concentration 2% w/v resulted in over seven times increase in the X1 yield (i.e. from 5.4 ± 0.1 to 40.3 ± 1.3 mg XOS/g xylan) and over two times increase in X2 yield (i.e. from 146.6 ± 2.6 to 306.9 ± 5.6 mg XOS/g xylan). Generating the rest of the linear XOS from X3 to X9 was also pH-dependent, with decreasing pH to ≤ 4.5 favouring their generation. Sing *et al.* studied the effect of pH, enzyme dose, and temperature on the enzymatic hydrolysis of pretreated arecanut husk using xylanase from *Trichoderma viride* (GH11), and showed the significant influence ($P < 0.05$) of pH on the XOS generation with the maximum amount of X2-X4 obtained at pH 4.0 (Singh et al., 2018).

In addition, the longest reaction time favoured the production of X1 over X2 as the enzyme had longer time to depolymerise the xylan and the initially longer XOS into shorter chains. Similar behaviour was reported previously in which endoxylanase from *Aspergillus oryzae* (GH11) was used to hydrolyse alkali pretreated corncob (Aachary and Prapulla, 2009).

It was also observed that the yield of low DP XOS, increased with increasing temperature. The temperature at which xylanase is active has been reported to range between 30 °C up to 75 °C (Singh et al., 2019), showing a peak activity at ~ 50 °C (Rahmani et al., 2019) as observed in the current study. Besides, it can be hypothesised that at higher temperature, the viscosity of the reaction medium decreases, enabling a better interaction of the substrate and enzyme (Linares-Pasten et al., 2017). Here, the generation of X1, X2MeGluA-X5MeGluA, and X7MeGluA2 became dominant when the hydrolysis was conducted at 50 °C, as the enzyme had better access to the xylan chains, converting them into low DP XOS.

3.2.2. Validation of the response surface methodology models

Quantitative experimental results were obtained following the optimum parameters suggested by the models for X1-X6 and used to validate the developed RSM models (Fig. 1A). The model predicted the maximum yield of X1 at pH 7.0, temperature 50 °C, reaction time 90 min, enzyme dose 75 U/mL, and xylan concentration 3% w/v. The X2 generation was favoured at the same pH, enzyme dose, and xylan concentration but at a temperature of 25 °C and a reaction time of 30 min. The predicted yield for X1 and X2 were 36.3 and 311.7 mg/g of xylan, respectively, which are very close to the 32.8 ± 1.8 mg X1/g of xylan and 314.2 ± 1.2 mg X2/g of xylan obtained experimentally.

Since the xylanase activity can be inhibited at high X1 concentration (Hegazy et al., 2018), its generation needs to be minimised when high DP XOS is desired. To minimise X1 generation, the RSM model predicted the following parameters: pH 4.6, temperature 25 °C, reaction time 30 min, enzyme dose 60 U/mL, and xylan concentration 3% w/v. According to the model, the predicted X1 yield, using these enzymatic hydrolysis parameters, was expected to be around zero which is once again very close to the 1.3 ± 0.1 mg/g xylan obtained experimentally.

The maximum yield for X3 predicted by the model was 92.6 mg/g of xylan, which is higher than but similar to the 76.6 ± 4.5 mg/g of xylan experimentally obtained at pH 4.5, temperature 25 °C, reaction time 30 min, enzyme dose 75 U/mL, and xylan concentration 3% w/v. For X4-X6, the RSM models predicted the maximum yields to be obtained at the same conditions of pH 4.0, temperature 25 °C, reaction time 30 min,

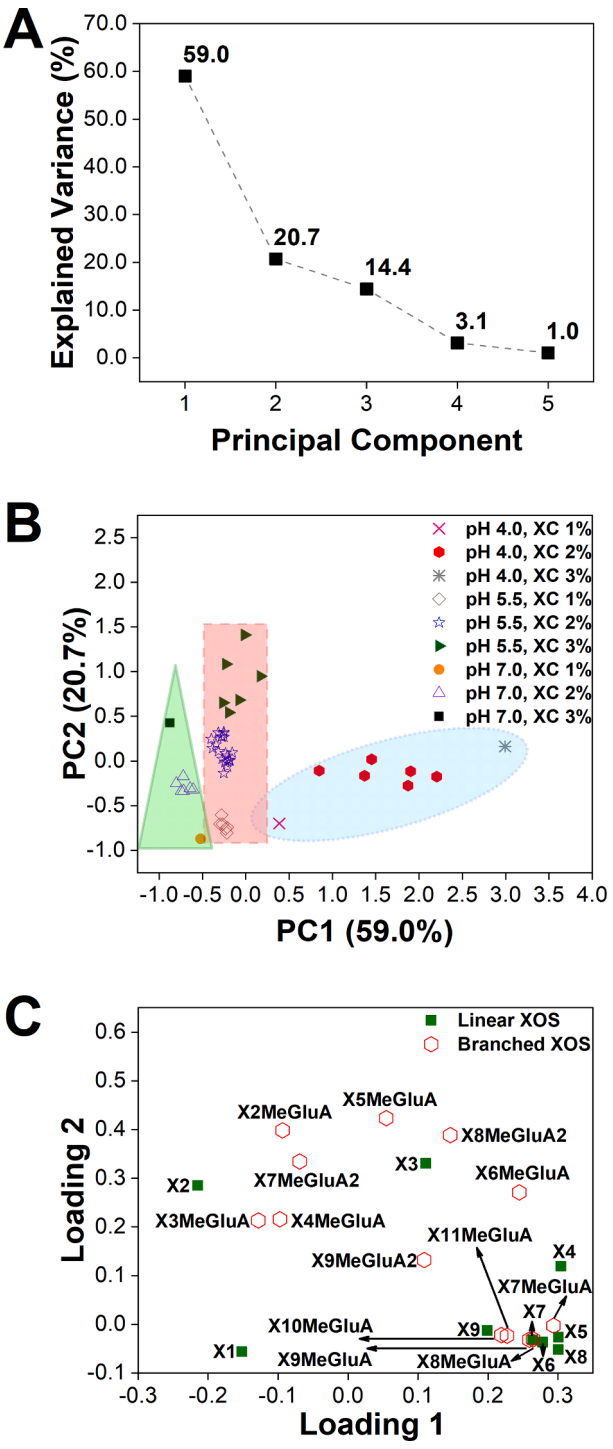

Fig. 2. Principal component analysis (PCA) of hydrolysate samples obtained using different hydrolysis parameters (A) Scree plot, (B) Scores plot (XC: xylan concentration, % w/v), and (C) Loading plot depicting the 22 XOS identified.

enzyme dose 75 U/mL, and xylan concentration 3% w/v. The predicted values were 43.0, 16.3, and 4.9 mg/g of xylan which map closely to the experimental values obtained, namely 38.4 ± 0.4, 17.8 ± 0.7, and 5.3 ± 0.2 mg/g of xylan, respectively.

To verify the agreement of the experimental values with those predicted by the RSM models, the Bland-Altman plot (Fig. 1B) was developed. In this figure, the line of equality is within the 95% confidence interval of the bias line, with all the points within the upper and lower limit of agreements. This indicates that the differences between the values obtained by the experimental and computational techniques were not statistically significant ($P > 0.05$), confirming the validity of the models (Haghayegh et al., 2020). Except for X3, for which the deviation of the experimental and predicted yields was ~ 18%, the differences observed for all X1 to X6, were < 10%, which is highly acceptable for such a complex biological system.

3.3. Principal component analysis

The RSM technique was used to investigate the hydrolysis parameters required to maximise/minimise the amount of the 22 XOS identified. To expand on the investigation and explore the correlation between XOS generated and the hydrolysis parameters, principal component analysis (PCA) was conducted. PCA is a technique that assists in interpreting large data sets by reducing their dimensionality while minimizing the loss of information (Jolliffe and Cadima, 2016). This pattern recognition technique facilitates the visualisation of patterns among samples in a reduced dimensional space (two or three-dimensional plots) (Lebanov et al., 2020). The first step in PCA is to identify the optimal number of variables, now called principal components (PCs), that capture a certain percentage of the total variance among the samples. The variance represented by each PC is plotted in descending order creating a Scree plot, as presented in Fig. 2A. In this figure, an "elbow" can be observed between the second and the third PCs. Further, by inspecting PCs 3–5, no correlation with other hydrolysis parameters is observed. Therefore, the first two PCs were retained in the PCA.

The scores plot in Fig. 2B shows the PC1 and PC2 clustered the hydrolysate samples based on pH and xylan concentration, respectively. PC1 accounts for 59.9% of the total variance of the dataset, while PC2 accounts for 20.7%. The total variance explained by PC1 and PC2 is therefore around 80%. The triangular cluster at negative scores of PC1 contains the samples obtained at high pH (7.0), while the oval cluster at positive scores contains the samples from low pH (4.0). For PC2, the positive and negative scores refer to the samples generated at high (3% w/v) and low (1% w/v) xylan concentrations, respectively. The rectangular cluster located close to the origin of PC1 and PC2 represents the samples generated at the medium level of both, pH (5.5) and xylan concentration (2% w/v).

The loading plot in Fig. 2C shows the 22 XOS identified in relation to pH (loading 1) and xylan concentration (loading 2). This figure reveals that the change in pH from 7.0 to 4.0, and xylan concentration from 3% to 1% w/v affected the resulting XOS profile. Samples produced at pH 7.0 favour the production of X1 and X2, branched X2MeGluA to X4MeGluA, and X7MeGluA2 (negative loadings of PC1). However, it is at pH 4.0 that all 22 XOS identified are consistently produced, including the linear X4 to X9, branched X6MeGluA to X11MeGluA, and X8MeGluA2 to X9MeGluA2 (positive loadings of PC1).

The highest yield of X1-X4 obtained in this study was 379.5 ± 5.6 mg XOS/g of xylan obtained at pH 7.0, 25 °C, 2% w/v xylan, enzyme dose 62.5 U/mL, and 60 min. This is comparable to the 372 mg of X1-X4/g of xylan reported by Singh *et al.* (Singh et al., 2018). In addition, the highest yields for DP 1–6 and DP 2–6 were 295.8 ± 3.9 and 291.7 ± 4.1 mg XOS/g xylan, respectively obtained at pH 4.0, 37.5 °C, 1% w/v xylan, enzyme dose 62.5 U/mL, and 60 min. These results are comparable with the ~ 350 mg of X2-X6/g of xylan reported by Rahmani *et al.* (Rahmani et al., 2019) and the 300 mg of X1-X6/g of pretreated sugarcane reported by Bragatto *et al.* (Bragatto et al., 2013). Bragatto *et al.* studied the production of XOS from pretreated sugarcane bagasse using xylanase extracted from *Bacillus subtilis* (GH11) (Bragatto et al., 2013). However, using HPAE coupled to pulsed amperometric detection (PAD), the identification of linear XOS with DP between 2 and 11 could only be achieved. Herein, identification of a larger number of XOS compounds ranging from linear XOS with DP from 1 to 9, and branched XOS with DP from 2 to 11 was achieved using HPAEC-QqQ-MS, showing the clear advantages to coupling suppressed HPAEC and MS compared with standard PAD detection. Most notably, the ability to detect and quantify

co-eluting species, and to confirm the identity of target solutes and unknowns, via their individual mass spectra (Vékey, 2001).

4. Conclusion

Combining chemometrics with HPAEC-QqQ-MS has been shown to be a powerful tool to characterise and tailor XOS production. Evaluating key parameters involved in the enzymatic hydrolysis of xylan including pH, temperature, substrate concentration, enzyme dosage, and reaction time, confirmed pH as the dominant factor influencing xylan hydrolysate yield and composition. Any combination of parameters that included low pH (4.0) resulted in a complete XOS profile, whereas higher pH (5.5 and 7.0) resulted in lower numbers of XOS. These results can be used to maximise the generation of desired XOS, enabling their commercial production by reducing the cost of downstream purification.

CRediT authorship contribution statement

Gloria Lizeth Díaz-Arenas: Conceptualization, Investigation, Formal analysis, Data curation, Writing – original draft. **Leo Lebanov:** Methodology, Formal analysis, Writing – review & editing. **Estrella Sanz Rodríguez:** Formal analysis, Writing – review & editing. **M. Munir Sadiq:** Writing – review & editing. **Brett Paull:** Resources, Writing – review & editing. **Gil Garnier:** Funding acquisition, Writing – review & editing. **Joanne Tanner:** Supervision, Writing – review & editing.

Declaration of Competing Interest

The authors declare that they have no known competing financial interests or personal relationships that could have appeared to influence the work reported in this paper.

Acknowledgements

The authors wish to express their gratitude to ARC Industrial Transformation Research Hub for Processing Advanced Lignocellulosics Products (PALs) grant for this research (Grant: ARC IH170100020). The funding from the Australian Government Research Training Program (RTP) Scholarship to G. L. Díaz-Arenas is greatly appreciated. The authors are also grateful to the Department of Chemical and Biological Engineering of Monash University and the School of Natural Sciences of the University of Tasmania. The authors acknowledge Thermo Fisher Scientific for placement of the IC-QqQ-MS instrument within the University of Tasmania to undertake this work. The authors would also like to acknowledge Dr M. Naseri for the provision of technical support.

Appendix A. Supplementary data

Supplementary data to this article can be found online at https://doi.org/10.1016/j.biortech.2022.127041.

References

Aachary, A.A., Prapulla, S.G., 2009. Value addition to corncob: Production and characterization of xylooligosaccharides from alkali pretreated lignin-saccharide complex using Aspergillus oryzae MTCC 5154. Bioresour. Technol. 100 (2), 991–995.

Aachary, A.A., Prapulla, S.G., 2011. Xylooligosaccharides (XOS) as an Emerging Prebiotic: Microbial Synthesis, Utilization, Structural Characterization, Bioactive Properties, and Applications. Compr. Rev. Food Sci. Food Saf. 10 (1), 2–16.

Akpinar, O., Ak, O., Kavas, A., Bakir, U., Yilmaz, L., 2007. Enzymatic Production of Xylooligosaccharides from Cotton Stalks. J. Agric. Food. Chem. 55 (14), 5544–5551.

Bhatia, R., Winters, A., Bryant, D.N., Bosch, M., Clifton-Brown, J., Leak, D., Gallagher, J., 2020. Pilot-scale production of xylo-oligosaccharides and fermentable sugars from Miscanthus using steam explosion pretreatment. Bioresour. Technol. 296, 122285.

Bowman, M.J., Dien, B.S., Hector, R.E., Sarath, G., Cotta, M.A., 2012. Liquid chromatography–mass spectrometry investigation of enzyme-resistant xylooligosaccharide structures of switchgrass associated with ammonia pretreatment, enzymatic saccharification, and fermentation. Bioresour. Technol. 110, 437–447.

Bragatto, J., Segato, F., Squina, F.M., 2013. Production of xylooligosaccharides (XOS) from delignified sugarcane bagasse by peroxide-HAc process using recombinant xylanase from Bacillus subtilis. Ind. Crops Prod. 51, 123–129.

Brenelli, L.B., Figueiredo, F.L., Damasio, A., Franco, T.T., Rabelo, S.C., 2020. An integrated approach to obtain xylo-oligosaccharides from sugarcane straw: From lab to pilot scale. Bioresour. Technol. 313, 123637.

Chadha, B.S., Kaur, B., Basotra, N., Tsang, A., Pandey, A., 2019. Thermostable xylanases from thermophilic fungi and bacteria: Current perspective. Bioresour. Technol. 277, 195–203.

Chapla, D., Pandit, P., Shah, A., 2012. Production of xylooligosaccharides from corncob xylan by fungal xylanase and their utilization by probiotics. Bioresour. Technol. 115, 215–221.

Ebringerová, A., 2005. Structural diversity and application potential of hemicelluloses. Macromol. Symp. Wiley Online Library 232 (1), 1–12.

Ghosh, D., Vir, A.B., Garnier, G., Patti, A.F., Tanner, J., 2021. Continuous flow production of xylooligosaccharides by enzymatic hydrolysis. Chem. Eng. Sci. 244, 116789.

Oliveira, M.G.d., Forte, M.B.S., Franco, T.T., 2021. A serial membrane-based process for fractionation of xylooligosaccharides from sugarcane straw hydrolysate. Sep. Purif. Technol. 278, 119285.

Guo, X., Fu, Y., Miao, F., Yu, Q., Liu, N.a., Zhang, F., 2020. Efficient separation of functional xylooligosaccharide, cellulose and lignin from poplar via thermal acetic acid/sodium acetate hydrolysis and subsequent kraft pulping. Ind. Crops Prod. 153, 112575.

Haghayegh, S., Kang, H.-A., Khoshnevis, S., Smolensky, M.H., Diller, K.R., 2020. A comprehensive guideline for Bland-Altman and intra class correlation calculations to properly compare two methods of measurement and interpret findings. Physiol. Meas. 41 (5), 055012.

Hegazy, U.M., El-Khonezy, M.I., Shokeer, A., Abdel-Ghany, S.S., Bassuny, R.I., Barakat, A.Z., Salama, W.H., Azouz, R.A.M., Fahmy, A.S., 2018. Revealing of a novel xylose-binding site of Geobacillus stearothermophilus xylanase by directed evolution. J. Biochem. 165 (2), 177–184.

Jolliffe, I.T., Cadima, J., 2016. Principal component analysis: a review and recent developments. Philos. Trans. Royal Soc. 374 (2065), 20150202.

Joshi, M.D., Hedberg, A., McIntosh, L.P., 2008. Complete measurement of the pKa values of the carboxyl and imidazole groups in Bacillus circulans xylanase. Protein Sci. 6 (12), 2667–2670.

Kabel, M.A., Schols, H.A., Voragen, A.G.J., 2002. Complex xylo-oligosaccharides identified from hydrothermally treated Eucalyptus wood and brewery's spent grain. Carbohydr. Polym. 50 (2), 191–200.

Kabel, M.A., Schols, H.A., Voragen, A.G.J., 2003. Identification of Structural Features of Various (*O*-Acetylated) Xylo-Oligosaccharides from Xylan-Rich Agricultural By-Products: A Review. Science and Technology. ACS Symp. Ser, Hemicelluloses, pp. 107–121.

Khuri, A.I., Mukhopadhyay, S., 2010. Response surface methodology. Wiley Interdiscip. Rev. Comput. Stat. 2 (2), 128–149.

Kucheryavskiy, S., 2020. mdatools – R package for chemometrics. Chemometrics Intellig. Lab. Syst. 198, 103937.

Lebanov, L., Tedone, L., Ghiasvand, A., Paull, B., 2020. Characterisation of complex perfume and essential oil blends using multivariate curve resolution-alternating least squares algorithms on average mass spectrum from GC-MS. Talanta 219, 121208.

Lenth, R.V., 2009. Response-Surface Methods in R. Using rsm. J. Stat. Softw. 32 (7), 1–17.

Li, H., Chen, X., Xiong, L., Luo, M., Chen, X., Wang, C., Huang, C., Chen, X., 2019. Stepwise enzymatic hydrolysis of alkaline oxidation treated sugarcane bagasse for the co-production of functional xylo-oligosaccharides and fermentable sugars. Bioresour. Technol. 275, 345–351.

Li, H., Chen, X., Xiong, L., Zhang, L., Chen, X., Wang, C., Huang, C., Chen, X., 2020. Production, separation, and characterization of high-purity xylobiose from enzymatic hydrolysis of alkaline oxidation pretreated sugarcane bagasse. Bioresour. Technol. 299, 122625.

Li, H., Xue, Y., Wu, J., Wu, H., Qin, G., Li, C., Ding, J., Liu, J., Gan, L., Long, M., 2016. Enzymatic hydrolysis of hemicelluloses from Miscanthus to monosaccharides or xylo-oligosaccharides by recombinant hemicellulases. Ind. Crops Prod. 79, 170–179.

Linares-Pasten, J.A., Aronsson, A., Karlsson, E.N., 2017. Structural Considerations on the Use of Endo-Xylanases for the Production of prebiotic Xylooligosaccharides from Biomass. Curr. Protein Peptide Sci. 19 (1), 1-1.

Mechelke, M., Herlet, J., Benz, J.P., Schwarz, W.H., Zverlov, V.V., Liebl, W., Kornberger, P., 2017. HPAEC-PAD for oligosaccharide analysis—novel insights into analyte sensitivity and response stability. Anal. Bioanal. Chem. 409 (30), 7169–7181.

Moniz, P., Pereira, H., Duarte, L.C., Carvalheiro, F., 2014. Hydrothermal production and gel filtration purification of xylo-oligosaccharides from rice straw. Ind. Crops Prod. 62, 460–465.

Moure, A., Gullón, P., Domínguez, H., Parajó, J.C., 2006. Advances in the manufacture, purification and applications of xylo-oligosaccharides as food additives and nutraceuticals. Process Biochem. 41 (9), 1913–1923.

Naidu, D.S., Hlangothi, S.P., John, M.J., 2018. Bio-based products from xylan: A review. Carbohydr. Polym. 179, 28–41.

Pang, Z., Chong, J., Zhou, G., David, A., Chang, L., Barrette, M., Gauthier, C., Jacques, P.-É., Li, S., Xia, J., 2021. MetaboAnalyst 5.0: narrowing the gap between raw spectra and functional insights. Nucleic Acids Res. 49 (W1), W388–W396.

Polizeli, M., Rizzatti, A., Monti, R., Terenzi, H., Jorge, J.A., Amorim, D., 2005. Xylanases from fungi: properties and industrial applications. Appl. Microbiol. Biotechnol. 67 (5), 577–591.

Rahmani, N., Kahar, P., Lisdiyanti, P., Lee, J., Yopi, Prasetya, B., Ogino, C., Kondo, A., 2019. GH-10 and GH-11 Endo-1,4-β-xylanase enzymes from Kitasatospora sp. produce xylose and xylooligosaccharides from sugarcane bagasse with no xylose inhibition. Bioresour. Technol. 272, 315–325.

Reis, A., Pinto, P., Evtuguin, D.V., Neto, C.P., Domingues, P., Ferrer-Correia, A.J., Domingues, M.R.M., 2005. Electrospray tandem mass spectrometry of underivatised acetylated xylo-oligosaccharides. Rapid Commun. Mass Spectrom. 19 (23), 3589–3599.

Rocklin, R.D., Pohl, C.A., 1983. Determination of carbohydrates by anion exchange chromatography with pulsed amperometric detection. J. Liq. Chromatogr. 6 (9), 1577–1590.

Samanta, A.K., Jayapal, N., Jayaram, C., Roy, S., Kolte, A.P., Senani, S., Sridhar, M., 2015. Xylooligosaccharides as prebiotics from agricultural by-products: Production and applications. Bioact. Carbohydr. Diet. Fibre 5 (1), 62–71.

Santibáñez, L., Henríquez, C., Corro-Tejeda, R., Bernal, S., Armijo, B., Salazar, O., 2021. Xylooligosaccharides from lignocellulosic biomass: A comprehensive review. Carbohydr. Polym. 251, 117118.

Sanz Rodríguez, E., Díaz-Arenas, G.L., Makart, S., Ghosh, D., Patti, A.F., Garnier, G., Tanner, J., Paull, B., 2022. Determination of xylooligosaccharides produced from enzymatic hydrolysis of beechwood xylan using high-performance anion-exchange chromatography tandem mass spectrometry. J. Chromatogr. A 1666, 462836.

Sanz Rodriguez, E., Perron, M.M.G., Strzelec, M., Proemse, B.C., Bowie, A.R., Paull, B., 2020. Analysis of levoglucosan and its isomers in atmospheric samples by ion chromatography with electrospray lithium cationisation - Triple quadrupole tandem mass spectrometry. J. Chromatogr. A 1610, 460557.

Singh, R.D., Banerjee, J., Sasmal, S., Muir, J., Arora, A., 2018. High xylan recovery using two stage alkali pre-treatment process from high lignin biomass and its valorisation to xylooligosaccharides of low degree of polymerisation. Bioresour. Technol. 256, 110–117.

Singh, S., Sidhu, G.K., Kumar, V., Dhanjal, D.S., Datta, S., Singh, J., 2019. Fungal Xylanases: Sources, Types, and Biotechnological Applications, Recent Advancement In White Biotechnology Through Fungi: Volume 1: Diversity And Enzymes Perspectives. Springer, Germany, pp. 405–428.

Sluiter, A., Hames, B., Ruiz, R., Scarlata, C., Sluiter, J., Templeton, D., Crocker, D., 2008. Determination of Structural Carbohydrates and Lignin in Biomass. Nat. Renew, Energy Lab.

Soliman, M.E.S., Ruggiero, G.D., Pernía, J.J.R., Greig, I.R., Williams, I.H., 2009. Computational mutagenesis reveals the role of active-site tyrosine in stabilising a boat conformation for the substrate: QM/MM molecular dynamics studies of wild-type and mutant xylanases. Org. Biomol. Chem. 7 (3), 460–468.

Sutay Kocabaş, D., Erkoç Akçelik, M., Bahçegül, E., Özbek, H.N., 2021. Bulgur bran as a biopolymer source: Production and characterization of nanocellulose-reinforced hemicellulose-based biodegradable films with decreased water solubility. Ind. Crops Prod. 171, 113847.

Taghvaei, M., Jafari, S.M., 2015. Application and stability of natural antioxidants in edible oils in order to substitute synthetic additives. J. Food Sci. Technol. 52 (3), 1272–1282.

Valls, C., Pastor, F.I.J., Vidal, T., Roncero, M.B., Díaz, P., Martínez, J., Valenzuela, S.V., 2018. Antioxidant activity of xylooligosaccharides produced from glucuronoxylan by Xyn10A and Xyn30D xylanases and eucalyptus autohydrolysates. Carbohydr. Polym. 194, 43–50.

Vékey, K., 2001. Mass spectrometry and mass-selective detection in chromatography. J. Chromatogr. A 921 (2), 227–236.

Wei, L., Liu, L., Bian, Z., Wu, Y., 2021. MALDI-TOF-MS analysis of hydrolysis products of beechwood and birchwood xylans catalyzed by xylanase from Bacillus subtilis. J. Food Biochem. 45 (8).

Xu, H., Zhang, F., Shang, H., Li, X., Wang, J., Qiao, D., Cao, Y., 2013. Alkalophilic adaptation of XynB endoxylanase from Aspergillus niger via rational design of pKa of catalytic residues. J. Biosci. Bioeng. 115 (6), 618–622.